Journal of Materials Chemistry A

PAPER

View Article Online
View Journal | View Issue

Published on 06 December 2013. Downloaded by Xiamen University on 11/12/2014 01:43:32.

Cite this: J. Mater. Chem. A, 2014, 2, 6191

A multiple coating route to hollow carbon spheres with foam-like shells and their applications in supercapacitor and confined catalysis†

Xiaoliang Fang,*[a] Jun Zang,[b] Xingli Wang,[bc] Ming-Sen Zheng[b] and Nanfeng Zheng*[bcd]

Received 25th November 2013
Accepted 5th December 2013

DOI: 10.1039/c3ta14881e

www.rsc.org/MaterialsA

Recent advances in the sol–gel process derived resorcinol-formaldehyde (RF) coating strategies offer new opportunities for the synthesis and applications of hollow carbon spheres (HCS). Due to the lack of an effective route for controlling the pore structures, the synthesis of RF resin derived HCS with a high specific surface area for promising applications is still a challenge. In this work, we present a facile and effective template-directed multiple coating route to synthesize RF resin derived HCS with foam-like shells (HCSF). The as-synthesized HCSF exhibit a significantly higher specific surface area (1286 $m^2\ g^{-1}$) and larger pore volumes (2.25 $cm^3\ g^{-1}$) than the RF resin derived HCS (639 $m^2\ g^{-1}$ and 0.56 $cm^3\ g^{-1}$). Our experiments demonstrated that the cationic surfactant CTAB plays a critical role in forming the foam-like pore structure. Compared with the RF resin derived HCS, the as-synthesized HCSF show advantageous performances in supercapacitor and confined catalysis due to their unique pore structures.

Introduction

Hollow carbon spheres (HCS) have attracted considerable attention because of their promising applications in catalysis,[1,2] lithium-ion batteries,[3–6] fuel cells,[2,7] supercapacitors,[8,9] and water treatment.[10] To upgrade their performance, HCS with high specific surface areas have been intensively pursued over the past decade.[11–14] In previous studies, the impregnation of the carbon precursors into a core–shell structured mesoporous silica (*i.e.* nanocasting) was a general route to synthesize HCS with a high specific surface area (>1000 $m^2\ g^{-1}$).[15,16] Due to the time-consuming synthetic procedures for preparing the core–shell structured templates, much effort has been devoted to the synthesis of HCS by the SiO_2-based hard-templating approach.[17–19] Some carbon sources, such as glucose, saccharine, and dopamine have been successfully employed to coat SiO_2 spheres with a layer of a carbon precursor, so that HCS can be obtained after carbonization and removal of SiO_2.[17–19]

Recent advances in the sol–gel polymerization of resorcinol (R) and formaldehyde (F) in a mixture of ethanol and aqueous ammonia infused new vitality into the design and synthesis of carbon nanomaterials.[20–23] RF resins have emerged as highly fascinating and versatile carbon precursors for the designed synthesis of HCS.[20–25] Although such a sol–gel process is very similar to that of SiO_2 spheres obtained by the Stöber method, the surface incompatibility of the RF resin with SiO_2 spheres make it difficult to utilize the SiO_2-templating methods to synthesize RF resin derived HCS.[26] To overcome this problem, our group and several other groups, recently developed cationic surfactant assisted RF resin coating strategies.[26–28] However, similar to the HCS obtained using glucose, saccharine, or dopamine as carbon sources, the reported RF resin derived HCS usually exhibit a relatively low specific surface area (~several hundred $m^2\ g^{-1}$) and low pore volumes (<1 $cm^3\ g^{-1}$).[26–28] From the viewpoint of practical applications, HCS with a high specific surface and large pore volumes are desirable to many surface-related applications, such as adsorption, supercapacitors, and lithium–sulfur batteries. Therefore, the design of a new and facile route to fabricate dispersible HCS with a high specific surface area and larger pore volumes is still a challenge.

Herein, we report a simple and effective multiple coating route to synthesize HCS with foam-like shells (HCSF) that have a high specific surface area and large pore volumes. Based on the modified cetyltrimethyl ammonium bromide (CTAB) assisted RF coating strategies, HCSF were successfully obtained from the sandwich-like SiO_2@RF/CTAB@SiO_2 spheres. As the carbonization process of the carbon precursor RF/CTAB is confined in

[a]Pen-Tung Sah Institute of Micro-Nano Science and Technology, Xiamen University, Xiamen 361005, China. E-mail: x.l.fang@xmu.edu.cn

[b]Department of Chemistry, Xiamen University, Xiamen 361005, China

[c]State Key Laboratory for Physical Chemistry of Solid Surfaces, Xiamen University, Xiamen 361005, China

[d]Collaborative Innovation Center of Chemistry for Energy Materials, Xiamen University, Xiamen 361005, China. E-mail: nfzheng@xmu.edu.cn

† Electronic supplementary information (ESI) available: The EDX spectrum of HCSF, TG curve of HCSF obtained under air atmosphere, TEM images of HCSF obtained at 700 °C and 900 °C, TEM images of the intermediates obtained in the carbonization of SiO_2@RF/CTAB@SiO_2 at different heating stages (350 °C and 550 °C), TEM image of Au@HCS, UV-vis spectrum of 4-nitrophenol, and UV-vis spectra for the adsorption of 4-nitrophenol by Au@HCSF and Au@HCS, respectively. See DOI: 10.1039/c3ta14881e

Published on 06 December 2013. Downloaded by Xiamen University on 11/12/2014 01:43:32.

the sandwich-like core–shell structures, the as-synthesized HCSF are highly dispersible in solution. By investigating the roles of CTAB, a formation process of the HCSF was proposed. Moreover, the proposed synthetic strategy can be extended as an effective route to synthesize yolk–shell structured HCSF, with functional nanoparticles. The as-synthesized HCSF and yolk–shell structured HCSF were applied in supercapacitors, and confined catalysis, respectively. Compared with the HCS, the enhanced performances of the HCSF make the proposed synthetic strategy an effective route to upgrade the performances of HCS.

Experimental

Chemicals

Tetraethyl orthosilicate (TEOS) and resorcinol were purchased from Alfa Aesar; aqueous ammonia solution (25–28%), CTAB, ethanol, formaldehyde, Rhodamine B (RhB), $HAuCl_4 \cdot 3H_2O$, sodium citrate, $NaBH_4$, and 4-nitrophenol were purchased from the Sinopharm Chemical Reagent Co. (Shanghai, China); PVP10 was purchased from Sigma-Aldrich. All the reagents were used without further purification. Deionized water was used in all the experiments.

Synthesis of SiO_2 spheres

The SiO_2 spheres were prepared following a slightly modified Stöber process. In a typical synthesis, 6 mL of TEOS was rapidly added to a mixture of 75 mL of ethanol, 10 mL of deionized water, and 3.15 mL of aqueous ammonia solution, and then stirred at room temperature for 1 h. The SiO_2 spheres were centrifugally separated from the suspension and washed with deionized water and ethanol.

Synthesis of SiO_2@RF/CTAB core–shell spheres

1 g of the SiO_2 spheres were homogeneously dispersed in a mixture of deionized water and ethanol by ultrasonication, followed by the addition of CTAB, and then stirring at room temperature. The mixed solution was homogenized for 20 min to form a uniform dispersion. Resorcinol and formaldehyde were added to the dispersion with continuous stirring for 10 min. After the addition of aqueous ammonia solution, the weight ratio of the SiO_2–CTAB–resorcinol–formaldehyde–H_2O–ethanol–ammonia solution was 1 : 1.5 : 0.32 : 0.49 : 600 : 197 : 3.64. The final mixture was stirred at 30 °C for 16 h, and the products SiO_2@RF/CTAB were collected by centrifugation.

Synthesis of HCS

The SiO_2@C core–shell spheres were obtained by the carbonization of the as-synthesized SiO_2@RF/CTAB core–shell spheres under a N_2 atmosphere at 350 °C, for 2 h, with a heating rate of 1.5 °C min^{-1}, which was followed by a further treatment at 800 °C, for 4 h, with a heating rate of 1.5 °C min^{-1}. After washing in a 4 M NaOH aqueous solution for 24 h, the as-synthesized SiO_2@C core–shell spheres were converted into the HCS.

Synthesis of HCSF

1.5 g of the SiO_2@RF/CTAB core–shell spheres were homogeneously dispersed in a mixture of 75 mL of ethanol, 10 mL of deionized water, and 3.15 mL of aqueous ammonia solution by ultrasonication. Then, 0.5 mL of TEOS was added under vigorous stirring every 0.5 h, up to a total TEOS volume of 3 mL. The resultant SiO_2@RF/CTAB@SiO_2 core–shell spheres were collected by centrifuging and then cleaned three times with water and ethanol. After the carbonization and removal of silica, according to the synthesis of the HCS, the as-synthesized SiO_2@RF/CTAB@SiO_2 core–shell spheres were converted into the HCSF.

Synthesis of Au@HCSF yolk–shell structures

Monodisperse gold nanoparticles were synthesized according to the standard sodium citrate reduction method. Briefly, 18.0 mg of $HAuCl_4 \cdot 3H_2O$ was dissolved in 30 mL of water and heated to boiling under vigorous stirring. 1.0 mL (3.0 wt%) of sodium citrate aqueous solution was injected quickly into the above mixture and then refluxed for 30 min. After the solution was cooled down to room temperature, an aqueous solution of PVP10 (12.8 g L^{-1}, 0.235 mL) was added to the colloidal gold solution, to modify the surface of the gold nanoparticles to facilitate a silica coating. The solution was stirred for 24 h at room temperature. The PVP-modified gold nanoparticles were collected by centrifugation and re-dispersed in 2.0 mL water. For the silica coating, gold nanoparticles covered by PVP (1.0 mL) were added into a mixture of isopropanol (46 mL), H_2O (6.6 mL), and ammonia (1.28 mL). Then, 0.6 mL of TEOS was added under vigorous stirring every 6 h up to a total TEOS volume of 1.6 mL. The resultant Au@SiO_2 spheres were collected by centrifugation and then cleaned three times with water and ethanol.

100 mg of the Au@SiO_2 spheres were dispersed in a mixture of deionized water and ethanol by ultrasonication, followed by the addition of CTAB. The mixed solution was stirred at room temperature for 20 min. R and F were then added to the mixture with continuous stirring for 10 min. After the addition of aqueous ammonia solution, the weight ratio of the Au@SiO_2–CTAB–resorcinol–formaldehyde–H_2O–ethanol–ammonia solution was 1 : 1.5 : 0.32 : 0.49 : 600 : 197 : 3.64. The final mixture was stirred at room temperature 30 °C for 16 h, and the resultant Au@SiO_2@RF/CTAB core–shell spheres were collected by centrifugation. The as-synthesized Au@SiO_2@RF/CTAB spheres were then homogeneously dispersed in a mixture of 37 mL of ethanol, 5 mL of deionized water, and 1.5 mL of aqueous ammonia solution by ultrasonication. 0.2 mL of TEOS was added under vigorous stirring every 0.5 h up to a total TEOS volume of 0.6 mL. The resultant Au@SiO_2@RF/CTAB@SiO_2 spheres were collected by centrifugation and then cleaned three times with water and ethanol. After the carbonization and removal of silica, according to the synthesis of the HCS, the as-synthesized Au@SiO_2@RF/CTAB and Au@SiO_2@RF/CTAB@SiO_2 core–shell spheres were converted into Au@HCS and Au@HCSF, respectively.

 This journal is © The Royal Society of Chemistry 2014

Published on 06 December 2013. Downloaded by Xiamen University on 11/12/2014 01:43:32.

Adsorption properties

A RhB aqueous solution was used for the adsorption studies. In a typical experiment, 20 mg of the adsorbent sample were added to 50 mL of the RhB aqueous solution under magnetic stirring at room temperature. After 12 h, the solid and liquid were separated by high-speed centrifugation (8000 rpm) for 8 min. The RhB concentration in the remaining solution was finally measured by a UV-vis spectrophotometer.

Electrodes preparation and electrochemical measurements

The electrochemical performance of the synthesized hollow carbon nanomaterials was tested with a three-electrode system in a 1 M KOH aqueous electrolyte solution, at room temperature. A Hg/HgO electrode and Pt foil acted as the reference and counter electrode, respectively. The test electrode was prepared by loading the slurry consisting of 80 wt% active material, 10 wt% carbon black, and 10 wt% poly(vinylidene fluoride) (PVDF) (in *N*-methylpyrrolidone) on a nickel foam and dried at 80 °C, for 1.5 h, under a vacuum. The as-formed electrodes were then pressed at a pressure of 10 MPa and further dried in a vacuum oven at 60 °C overnight. The loading mass of the active materials on each current collector was 3.0 mg, and the area was 1.0 cm^2. Cyclic voltammetry curves were obtained in the potential range of −1.0–0 V *vs.* Hg/HgO by varying the scan rate from 2 to 200 mV s^{-1}. Charge–discharge measurements were carried out galvanostatically at 2–20 A g^{-1}, over a voltage range of −1.0–0 V *vs.* Hg/HgO.

Catalytic reduction of 4-nitrophenol with Au@HCSF

The Au@HCSF yolk–shell spheres with 2.5×10^{-4} mmol of Au cores were homogeneously dispersed in 5 mL of deionized water by ultrasonication, followed by the addition of 0.5 mL of $NaBH_4$ aqueous solution (0.5 M), and the mixture was stirred for 10 min at room temperature. 0.25 mL of 4-nitrophenol (0.12 M) was then added to the mixture, which was stirred until the deep yellow solution became colorless. During the course of the reaction, the reaction progress was monitored by measuring the UV-vis absorption spectra of the mixture.

Characterization

Scanning electron microscopy (SEM) and transmission electron microscopy (TEM) images were taken on a Hitachi S-4800 microscope with a field-emission electron gun and a TECNAI F-30 high-resolution transmission electron microscope operating at 300 kV. The energy-dispersive X-ray (EDX) spectrum of the HCSF was measured on a TECNAI F-30. The thermogravimetric (TG) analysis was carried out on a SDT-Q600. The surface area of the hollow carbon spheres were measured by the Brunauer–Emmett–Teller method, using nitrogen adsorption and desorption isotherms on a Micrometrics ASAP 2020 system. The pore size distribution plot was obtained by the Barrett–Joyner–Halenda method. The UV-vis spectra were recorded in the range of 210–800 nm with a Varian Cary 5000 spectrometer. All the electrochemical experiments were carried out on a CHI 760D electro-chemical workstation. The size distributions of the HCS and HCSF were measured from dynamic light scattering (DLS), using a Zetasizer (Nano ZS, Malvern).

Results and discussion

Synthesis and characterization of HCSF

Fig. 1a illustrates the general multiple coating route to synthesize the HCSF, based on a modified RF resin coating strategy. In a typical synthetic procedure, the R and F were used as the carbon sources and SiO_2 spheres, obtained by the Stöber method, were used as the templates. Based on our recent reported cationic surfactant assisted RF coating strategy, the core–shell structured SiO_2@RF/CTAB spheres were firstly synthesized by a convenient sol–gel process.[27] After the carbonization of the SiO_2@RF/CTAB spheres at 800 °C, under a N_2 atmosphere, and the subsequent removal of the templates SiO_2 by a NaOH aqueous solution, the routine HCS were obtained. For the synthesis of the HCSF, the SiO_2@RF/CTAB spheres were coated with a layer of the sol–gel, derived SiO_2, to form a sandwich-like SiO_2@RF/CTAB@SiO_2 spheres. After the same procedures according to the synthesis of the HCS, the SiO_2@RF/CTAB@SiO_2 spheres were successfully converted into HCSF. Based on the weights, the yields of the HCS and HCSF were calculated to be 40.2% and 45.6% related to the total weight of the reactants R and F, respectively. As shown in Fig. 1b–d, the TEM images of the SiO_2@RF/CTAB and SiO_2@RF/CTAB@SiO_2 spheres revealed their well-defined core–shell and sandwich-like structures, respectively.

The typical TEM images and SEM images show that the HCS have a uniform spherical morphology (Fig. 2a–c). The interior hollow size of the HCS agrees well with the diameter of the SiO_2 templates. The thickness of the carbon shells of the HCS (*ca.* 15 nm) is smaller than the thickness of the RF layer of the SiO_2@RF/CTAB spheres (*ca.* 50 nm), due to the shrinkage of the

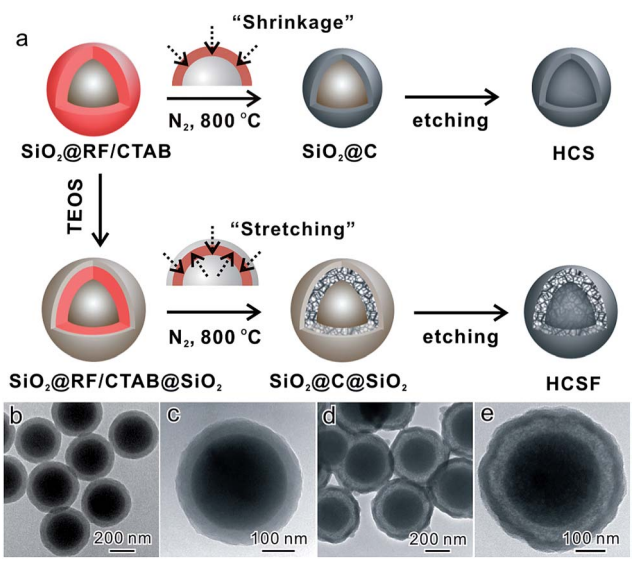

Fig. 1 (a) Schematic illustration of selective synthesis of HCS and HCSF, (b and c) TEM images of SiO_2@RF/CTAB spheres, (d and e) TEM images of SiO_2@RF/CTAB@SiO_2 spheres.

Published on 06 December 2013. Downloaded by Xiamen University on 11/12/2014 01:43:32.

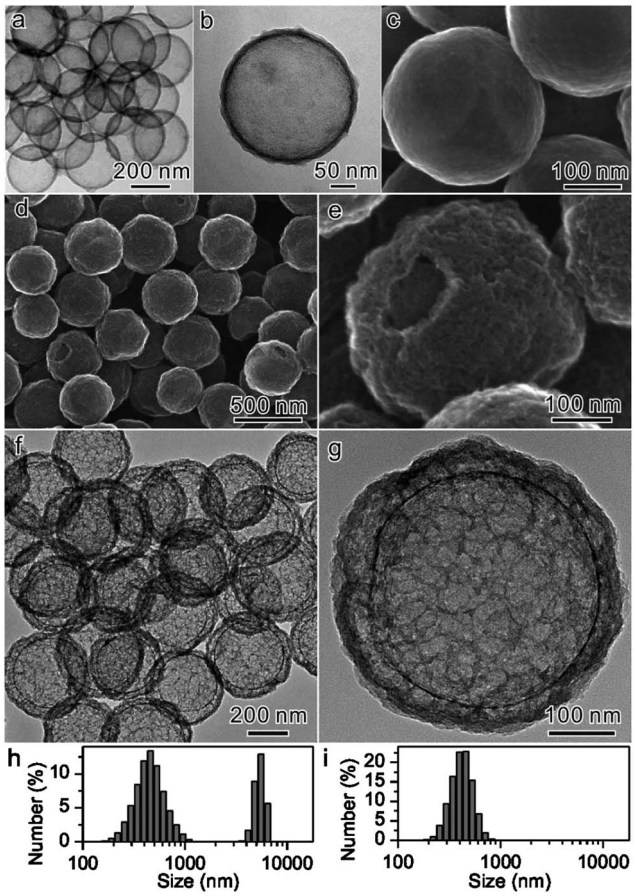

Fig. 2 (a and b) TEM images and (c) SEM image of HCS, (d and e) SEM images and (f and g) TEM images of HCSF obtained at 800 °C. (h) and (i) show the size distribution of HCS and HCSF particles dispersed in ethanol, respectively.

carbon precursor during the carbonization process at higher temperatures. Such an inevitable shrinkage is a general phenomenon in the routine synthesis of HCS.[17–19] The typical SEM image of the HCS (Fig. 2c) reveals that the surface of the HCS is smooth. Interestingly, different from the HCS, the HCSF are uniform corrugated spheres, with a coarse surface (Fig. 2d). The high-magnification SEM image of the HCSF further reveals that there are many nanopores running through the carbon shells of the HCSF (Fig. 2e). As shown in Fig. 2f, both the interior hollow size and the thickness of the carbon shells of the HCSF agree well with the diameter of the SiO_2 templates and the thickness of the RF/CTAB layer of the SiO_2@RF/CTAB@SiO_2 spheres, respectively. A typical TEM image (Fig. 2g) clearly indicates that the foam-like carbon shells of the HCSF exhibits a porous net-like structure, with pore sizes in the range of several nanometers to tens of nanometers. The EDX spectrum and TG curve of the HCSF reveal that both the SiO_2 templates and SiO_2 shells were completely removed by the alkaline etching (Fig. S1†). Furthermore, the TEM images of the HCSF, obtained at 700 °C and 900 °C (Fig. S2†), reveal that the HCSF obtained at different carbonization temperatures possess a similar morphology and pore structures. During the high-temperature carbonization, the as-synthesized HCS have a tendency to sinter, to form aggregated particles. Indeed, our DLS measurements showed that an ethanol dispersion of the HCS displayed this aggregation behavior, with the presence of some large particles, micrometers in size (Fig. 2h). In comparison, thanks to the structural feature that the carbon precursor layers in the SiO_2@RF/CTAB@SiO_2 spheres were separated by the SiO_2 shells, the as-synthesized HCSF are highly discrete and dispersible in ethanol (Fig. 2i). In previous reports, dispersible HCS are highly desirable in some potential applications, such as in catalysis and as drug carriers.[10]

Formation process of HCSF

To study the formation process of the HCSF, the carbonization of the SiO_2@RF/CTAB@SiO_2 spheres were monitored using TEM, by taking out samples at different heating stages. At 350 °C, no obvious porous structures were observed in the carbon precursor layers (Fig. S3†). With the temperature increased to 550 °C, porous structures started to appear in the carbon precursor layers. Also, the carbon precursor layers tended to migrate to the surface of the SiO_2 spheres and the inner surface of the SiO_2 shells (Fig. S4†). Based on the observed intermediates, of SiO_2@RF/CTAB@SiO_2, during the carbonization, we propose a formation process for the HCSF, in Fig. 1a. In the proposed process, CTAB plays an important role in forming the HCSF. During carbonization, the interface of the SiO_2 with RF/CTAB (designated as SiO_2–RF/CTAB) guides the shrinking directions of the carbon precursor layers. Without the SiO_2 shell, the RF/CTAB layers of the SiO_2@RF/CTAB spheres are shrunk towards the surface of the inner SiO_2 spheres during carbonization, resulting in the formation of the HCS with compact carbon shells. In comparison, there are two SiO_2–RF/CTAB interfaces in the SiO_2@RF/CTAB@SiO_2 system. As a result, the carbon precursor layers are shrunk towards two SiO_2–RF/CTAB interfaces (*i.e.*, SiO_2 cores–RF/CTAB and RF/CTAB–SiO_2 shells) to yield the foam-like mesoporous structures in the carbon precursor layers. More importantly, the confined space provided by the SiO_2 cores and the SiO_2 shells makes the thickness of the carbon shells of the HCSF agree well with the initial thickness of the RF/CTAB layer during the carbonization process. To further demonstrate the important role of the interface SiO_2–RF/CTAB, a control experiment was designed, by removing the CTAB from the RF/CTAB layers (Fig. 3a). After the removal of CTAB by extracting the SiO_2@RF/CTAB spheres with a mixture of hydrochloric acid and ethanol,[29] the as-synthesized SiO_2@RF spheres were further coated with SiO_2, resulting in the SiO_2@RF@SiO_2 spheres. As expected, in the absence of the interface SiO_2–RF/CTAB, the SiO_2@RF@SiO_2 spheres were converted into HCS, with a solid carbon shell rather than HCSF (Fig. 3b and c) after the same carbonization and SiO_2 removal processes.

Pore structures and adsorption performance of HCSF

As shown in Fig. 4a, the N_2 sorption isotherms clearly demonstrate the high porosity of the HCSF with a high nitrogen uptake, while the samples of HCS have a relatively low porosity.

 This journal is © The Royal Society of Chemistry 2014

Published on 06 December 2013. Downloaded by Xiamen University on 11/12/2014 01:43:32.

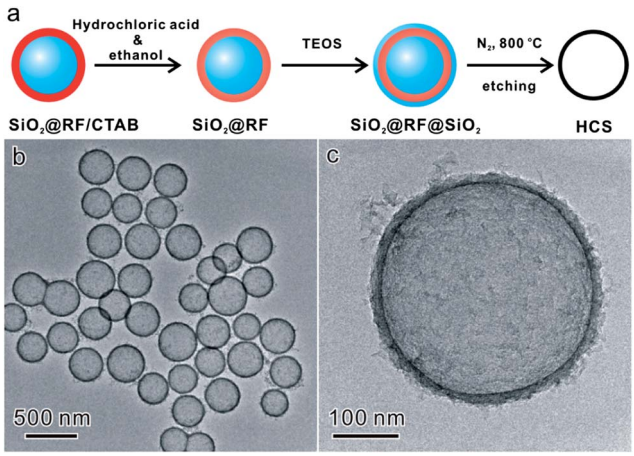

Fig. 3 (a) Schematic illustration of synthetic route for the control experiment, (b and c) TEM images of HCS obtained by SiO_2@RF@SiO_2.

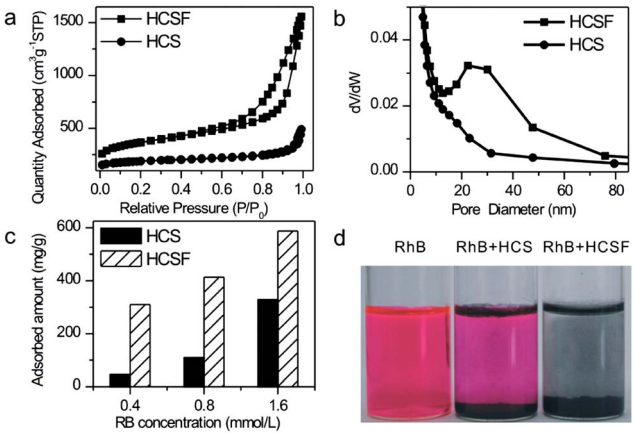

Fig. 4 (a and b) N_2 sorption isotherm and the pore size distribution of HCS and HCSF, (c) the maximal removal capacities of RhB on HCS and HCSF at different concentration of RhB aqueous solution, (d) the optical photographs for RhB aqueous solution (0.4 mmol L^{-1}) treated with HCS and HCSF, respectively.

The Brunauer–Emmett–Teller (BET) surface area and pore volumes of the HCS are 639 $m^2\ g^{-1}$ and 0.56 $cm^3\ g^{-1}$, respectively. In comparison, the HCSF exhibit a higher BET surface area (1286 $m^2\ g^{-1}$) and pore volumes (2.25 $cm^3\ g^{-1}$). We tried to optimize the carbonization temperature (800 °C) for the HCSF, based on the N_2 adsorption–desorption measurements. The BET surface areas of the HCSF, obtained at 700 and 900 °C are 978 $m^2\ g^{-1}$ and 868 $m^2\ g^{-1}$, respectively. As revealed by the pore size distributions of the HCS and HCSF obtained from the analysis of the adsorption branch of the isotherm using the Barrett–Joyner–Halenda method (Fig. 4b), the dominating pore, with diameters less than 2 nm, indicate the microporosity of the HCS. Compared with HCS, the mesoporous HCSF has a broad size distribution, centered at 30 nm, in good agreement with the TEM observation. With a high specific surface area and pore volumes, the HCSF are expected as promising candidates for potential applications.

Compared with the small molecule N_2, the penetration of a large molecule is very important to the practical applications of HCS, such as adsorption and the diffusion of an electrolyte or reactant molecule.[9,13] Consequently, we further used RhB as a probe molecule to evaluate the adsorption performances of the HCSF and HCS.[30] As shown in Fig. 4c, after treating the RhB aqueous solution with the as-synthesized HCS, the HCSF possesses a much higher removal capacity for RhB than HCS. At a low concentration of RhB (0.4 mmol L^{-1}), the adsorption capacities of the HCSF (328.8 mg L^{-1}) are about 7.1 times higher than the HCS (46.3 mg L^{-1}). When using the higher concentration of RhB (1.6 mmol L^{-1}), the adsorption capacities of HCSF (587.6 mg L^{-1}) are 1.9 times higher than the HCS (310.0 mg L^{-1}). The adsorption capacities of the HCSF are also higher than the commercial activated carbon.[30] For a direct observation, optical photographs were taken before and after the RhB adsorption (Fig. 4d). The RhB solution, with an initial concentration of 0.4 mmol L^{-1}, when treated with HCSF, became clear and colorless. In comparison, the solution treated with he HCS remained purple, indicating the incomplete removal of the RhB. The high adsorption capacities of the HCSF suggests that the mesoporous and permeable pore structures of the HCSF are available for other surface-related applications and the design of the functional HCSF composites, such as electrochemical energy storage[9,13] and yolk–shell structured nanoreactors.[1]

Electrochemical properties of HCSF

To demonstrate the HCSF as potential electrode materials for supercapacitors, the cyclic voltammetry (CV) and galvanostatic charge–discharge (CD) tests for HCSF and HCS were performed with a three-electrode cell, under the potential window of −1.0–0 V, employing a 1.0 M KOH solution as the electrolyte. Fig. 5a

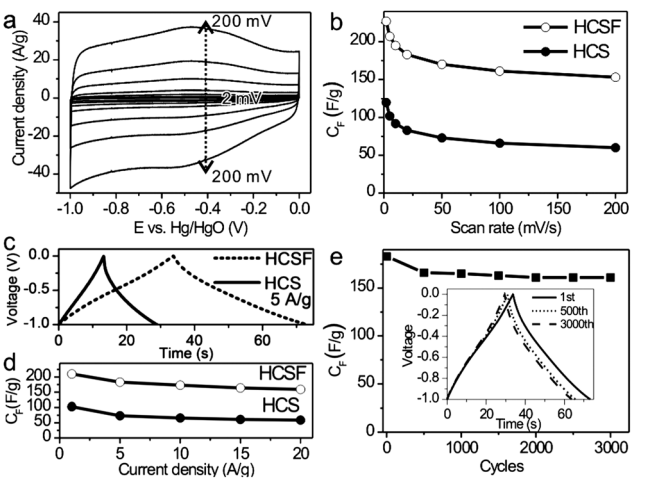

Fig. 5 (a) CV curves of HCSF at the scan rates from 2 to 200 mV s^{-1}, (b) the correlation of specific capacitances with scan rates for the HCSF and HCS, (c) typical CD curves of HCSF and HCS at a current density of 5 A g^{-1}, (d) the specific capacitances of HCSF and HCS calculated from CD curves *versus* discharge current density, (e) cycling performance of HCSF at a current density of 5 A g^{-1} (inset: CD curves of some typical charging–discharging cycles at a current density of 5 A g^{-1}).

Published on 06 December 2013. Downloaded by Xiamen University on 11/12/2014 01:43:32.

shows the CV curves of the HCSF, at scan rates from 2 to 200 mV s^{-1}. The CV curves exhibit quasi rectangular shapes, even at high scan rates, suggesting a typical electrical double layer capacitor behavior for the HCSF. The specific capacitances of the HCSF and HCS, calculated from the CV curves at a scan rate of 2 mV s^{-1}, are 227 F g^{-1} and 120 F g^{-1}, respectively (Fig. 5b). It is worth noting that the specific capacitance of the HCSF remains as high as 153 F g^{-1} at a scan rate of 200 mV s^{-1}, superior to our HCS (*ca.* 60 F g^{-1}) and the previously reported HCS and porous carbon materials.[23,31,32] The superior performance of the HCSF can be attributed to their high specific surface area and unique pore structure, which is beneficial for electrolyte penetration and accelerate the kinetic process of the ion transfer within the electrode materials.[33,34]

The typical CD curves and calculated specific capacitances *versus* discharge current densities are shown in Fig. 5c and d, respectively. The HCSF give a specific capacitance of up to 210 F g^{-1} at a current density of 1 A g^{-1}, and a specific capacitance of 159 F g^{-1} can be obtained even at a high current density of 20 A g^{-1} (Fig. 5d), much higher than the HCS (59 F g^{-1}). The electrochemical stability of the HCSF, at a current density of 5 A g^{-1} for 3000 cycles, is shown in Fig. 5e. The specific capacitances firstly drop by *ca.* 9.2%, from 183 to 165 F g^{-1}, during the first 500 cycles and then remain almost constant for the next 2500 cycles, indicating that the HCSF have a good electrochemical stability.[9]

Yolk–shell structured HCSF nanoreactor

It is well-known that the interior of hollow porous nanostructures decorated by catalytically active nanoparticles (*i.e.*, yolk–shell structures) have been demonstrated as ideal nanoreactors for confined catalysis, owing to their structural feature that the functional nanoparticles are isolated by the permeable shells.[1,35,36] Since the templates used in the proposed synthetic process are the sol–gel derived SiO_2 spheres, the yolk–shell structured HCSF with functional cores can be easily prepared by replacing the SiO_2 spheres with SiO_2-coated composites. For instance, when Au@SiO_2 core–shell spheres were used as templates, the well-defined yolk–shell structures with movable Au cores, nicely encapsulated in the HCSF shells (*i.e.*, Au@HCSF), were obtained (Fig. 6a and b). In order to demonstrate that the Au@HCSF nanoreactors can surpass their Au@HCS counterparts (Fig. S4†), the reduction of 4-nitrophenol by $NaBH_4$, to 4-aminophenol, was chosen as a model reaction to evaluate the catalytic performances of the Au@HCSF and Au@HCS.[37–39] The reduction process was monitored by UV-vis absorption spectroscopy (Fig. 6c). The reduction reaction did not proceed in the absence of the Au yolk–shell catalyst (Fig. 6d).[37–39] It is worth noting that the adsorption of the hydrophilic 4-nitrophenol on the hydrophobic Au@HCSF and Au@HCS can be ignored during the catalytic process (Fig. 6d and S4†). Furthermore, no byproducts were observed during the reaction (Fig. 6c).[37] Since this reduction reaction can be considered as a pseudo-first-order reaction,[37–39] the linear relation of $\ln(C_t/C_0)$ *versus* time, where C_t and C_0 are the 4-nitrophenol concentrations, at times t and 0, respectively, were observed for the Au@HCSF catalysts (Fig. 6d). The rate constants of the Au@HCSF and Au@HCS catalysts were calculated to be 0.085 min^{-1} and 0.065 min^{-1}, respectively. The higher rate constant of the Au@HCSF suggest that the mesoporous nature of the HCSF facilitates the diffusion of the reactants, even though the thickness of the HCSF shells in the Au@HCSF is larger than their microporous Au@HCS counterparts (Fig. S4†).[37]

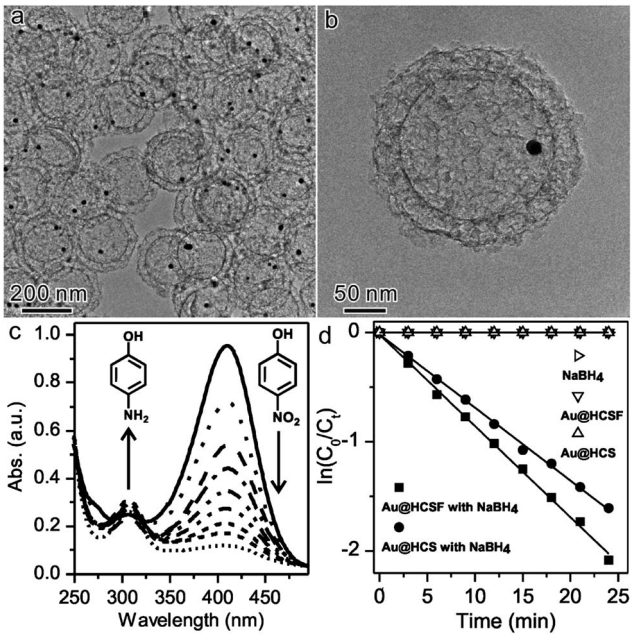

Fig. 6 (a and b) TEM images of Au@HCSF, (c) UV-vis spectra showing gradual reduction of 4-nitrophenol with Au@HCSF (d) plot of $\ln(C_t/C_0)$ *versus* time for the reduction of 4-nitrophenol into 4-aminophenol by $NaBH_4$, and Au@HCSF and Au@HCS catalytic nanoreactors with, or without $NaBH_4$, respectively.

Conclusions

In summary, we have demonstrated an effective route to synthesize HCSF, with high specific surface areas. Utilizing the good affinity of CTAB with RF and silica, to regulate the carbonization process, is critical to the formation of the HCSF. Our results demonstrate that the as-synthesized HCSF present preferable properties in adsorption, as supercapacitors, and in confined catalysis, compared with the routine HCS. Based on the unique characteristics of the HCSF, we believe that the developed synthetic strategy can be extended to produce new carbon composite nanomaterials with enhanced performances for other promising applications, such as catalyst supports, lithium-sulfur batteries,[40] and magnetically recyclable yolk–shell sorbents.

Acknowledgements

We thank the NSFC (21301144, 21131005, 21333008, 20925103, 21021061), and the MOST of China (2011CB932403), for their financial support.

 This journal is © The Royal Society of Chemistry 2014

Published on 06 December 2013. Downloaded by Xiamen University on 11/12/2014 01:43:32.

Notes and references

1 S. Ikeda, S. Ishino, T. Harada, N. Okamoto, T. Sakata, H. Mori, S. Kuwabata, T. Torimoto and M. Matsumura, *Angew. Chem., Int. Ed.*, 2006, **45**, 7063–7066.

2 Z. L. Schaefer, M. L. Gross, M. A. Hickner and R. E. Schaak, *Angew. Chem., Int. Ed.*, 2010, **49**, 7045–7048.

3 K. Tang, R. J. White, X. K. Mu, M. Titirici, P. A. V. Aken and J. Maier, *ChemSusChem*, 2012, **5**, 400–403.

4 N. Liu, H. Wu, M. T. McDowell, Y. Yao, C. Wang and Y. Cui, *Nano Lett.*, 2012, **12**, 3315–3321.

5 W.-M. Zhang, J.-S. Hu, Y.-G. Guo, S.-F. Zheng, L.-S. Zhong, W.-G. Song and L.-J. Wan, *Adv. Mater.*, 2008, **20**, 1160–1165.

6 K. T. Lee, Y. S. Jung and S. M. Oh, *J. Am. Chem. Soc.*, 2003, **125**, 5652–5653.

7 G. S. Chai, S. B. Yoon, J. H. Kim and J. S. Yu, *Chem. Commun.*, 2004, 2766–2767.

8 Z. B. Lei, Z. W. Chen and X. S. Zhao, *J. Phys. Chem. C*, 2010, **114**, 19867.

9 K. Xie, X. Qin, X. Wang, Y. Wang, H. Tao, Q. Wu, L. Yang and Z. Hu, *Adv. Mater.*, 2012, **24**, 347–352.

10 A. H. Lu, T. Sun, W. C. Li, Q. Sun, F. Han, D. H. Liu and Y. Guo, *Angew. Chem., Int. Ed.*, 2011, **50**, 11765–11768.

11 N. Jayaprakash, J. Shen, S. S. Moganty, A. Corona and L. A. Archer, *Angew. Chem., Int. Ed.*, 2011, **50**, 5904–5908.

12 S. Yang, X. Feng, L. Zhi, Q. Cao, J. Maier and K. Mullen, *Adv. Mater.*, 2010, **22**, 838–842.

13 C. F. Zhang, H. B. Wu, C. Z. Yuan, Z. Guo and X. W. Lou, *Angew. Chem., Int. Ed.*, 2012, **51**, 9592–9595.

14 M. Kim, B. Z. Fang, J. H. Kim, D. Yang, Y. K. Kim, T. S. Bae and J. S. Yu, *J. Mater. Chem.*, 2011, **21**, 19362–19367.

15 S. B. Yoon, K. Sohn, J. Y. Kim, C. H. Shin, J. S. Yu and T. Hyeon, *Adv. Mater.*, 2002, **14**, 19–21.

16 S. Ikeda, K. Tachi, Y. H. Ng, Y. Ikoma, T. Sakata, H. Mori, T. Harada and M. Matsumura, *Chem. Mater.*, 2007, **19**, 4335–4340.

17 R. J. White, K. Tauer, M. Antonietti and M. Titirici, *J. Am. Chem. Soc.*, 2010, **132**, 17360.

18 Y. Wan, Y. L. Min and S. H. Yu, *Langmuir*, 2008, **24**, 5024–5028.

19 R. Liu, S. M. Mahurin, C. Li, R. R. Unocic, J. C. Idrobo, H. Gao, S. J. Pennycook and S. Dai, *Angew. Chem., Int. Ed.*, 2011, **50**, 6799–6802.

20 J. Liu, S. Z. Qiao, H. Liu, J. Chen, A. Orpe, D. Zhao and G. Q. Lu, *Angew. Chem., Int. Ed.*, 2011, **50**, 5947–5951.

21 A. H. Lu, G. P. Hao and Q. Sun, *Angew. Chem., Int. Ed.*, 2011, **50**, 9023–9025.

22 A. B. Fuertes, P. Valle-Vigon and M. Sevilla, *Chem. Commun.*, 2012, **48**, 6124–6126.

23 Z. Qiao, B. K. Guo, A. J. Binder, J. H. Chen, G. M. Veith and S. Dai, *Nano Lett.*, 2013, **13**, 207–212.

24 T. Yang, J. Liu, Y. Zheng, M. J. Monteiro and S. Z. Qiao, *Chem.–Eur. J.*, 2013, **19**, 6942–6945.

25 Q. Sun, W. C. Li and A. H. Lu, *Small*, 2013, **9**, 2086–2090.

26 N. Li, Q. Zhang, J. Liu, J. Joo, A. Lee, Y. Gan and Y. Yin, *Chem. Commun.*, 2013, **49**, 5135–5137.

27 X. L. Fang, S. J. Liu, J. Zang, C. F. Xu, M. S. Zheng, Q. F. Dong, D. P. Sun and N. F. Zheng, *Nanoscale*, 2013, **5**, 6908–6916.

28 B. Guan, X. Wang, Y. Xiao, Y. Liu and Q. Huo, *Nanoscale*, 2013, **5**, 2469–2475.

29 D. Fujikawa, M. Uota, G. Sakai and T. Kijima, *Carbon*, 2007, **45**, 1289–1295.

30 X. Zhuang, Y. Wan, C. M. Feng, Y. Shen and D. Y. Zhao, *Chem. Mater.*, 2009, **21**, 706–716.

31 B. Liu, H. Shioyama, T. Akita and Q. Xu, *J. Am. Chem. Soc.*, 2008, **130**, 5390–5391.

32 Z. Fan, Y. Liu, J. Yan, G. Ning, Q. Wang, T. Wei, L. Zhi and F. Wei, *Adv. Energy Mater.*, 2012, **2**, 419–424.

33 D. W. Wang, F. Li, M. Liu, G. Q. Lu and H. M. Cheng, *Angew. Chem., Int. Ed.*, 2008, **47**, 373–376.

34 Y. P. Zhai, Y. Q. Dou, D. Y. Zhao, P. F. Fulvio, R. T. Mayes and S. Dai, *Adv. Mater.*, 2011, **23**, 4828.

35 P. M. Arnal, M. Comotti and F. Schüth, *Angew. Chem., Int. Ed.*, 2006, **45**, 8224–8227.

36 X. L. Fang, X. J. Zhao, W. J. Fang, C. Chen and N. F. Zheng, *Nanoscale*, 2013, **5**, 2205–2218.

37 J. Lee, J. C. Park and H. Song, *Adv. Mater.*, 2008, **20**, 1523–1528.

38 Q. Zhang, T. R. Zhang, J. P. Ge and Y. D. Yin, *Nano Lett.*, 2008, **8**, 2867–2871.

39 X. L. Fang, Z. H. Liu, M. F. Hsieh, M. Chen, P. X. Liu, C. Chen and N. F. Zheng, *ACS Nano*, 2012, **6**, 4434–4444.

40 C. F. Zhang, H. B. Wu, C. Z. Yuan, Z. P. Guo and X. W. Lou, *Angew. Chem., Int. Ed.*, 2012, **51**, 9592–9595.